PERGAMON

International Journal of Solids and Structures 40 (2003) 2589–2609

INTERNATIONAL JOURNAL OF SOLIDS and STRUCTURES

www.elsevier.com/locate/ijsolstr

A generalized self-consistent method accounting for fiber section shape

C.P. Jiang [a,b], Z.H. Tong [b], Y.K. Cheung [c,*]

[a] LNM, Institute of Mechanics, Chinese Academy of Sciences, Beijing 100080, PR China
[b] Solid Mechanics Research Center, Beijing University of Aeronautics and Astronautics, Beijing 100083, PR China
[c] Department of Civil Engineering, The University of Hong Kong, Hong Kong

Received 5 November 2001; received in revised form 7 October 2002

Abstract

A three-phase confocal elliptical cylinder model is proposed for fiber-reinforced composites, in terms of which a generalized self-consistent method is developed for fiber-reinforced composites accounting for variations in fiber section shapes and randomness in fiber section orientation. The reasonableness of the fiber distribution function in the present model is shown. The dilute, self-consistent, differential and Mori–Tanaka methods are also extended to consider randomness in fiber section orientation in a statistical sense. A full comparison is made between various micromechanics methods and with the Hashin and Shtrikman's bounds. The present method provides convergent and reasonable results for a full range of variations in fiber section shapes (from circular fibers to ribbons), for a complete spectrum of the fiber volume fraction (from 0 to 1, and the latter limit shows the correct asymptotic behavior in the fully packed case) and for extreme types of the inclusion phases (from voids to rigid inclusions). A very different dependence of the five effective moduli on fiber section shapes is theoretically predicted, and it provides a reasonable explanation on the poor correlation between previous theory and experiment in the case of longitudinal shear modulus.

Keywords: Generalized self-consistent method; Three-phase confocal elliptical cylinder model; Effective moduli; Micromechanics of composites; Conformal mapping technique

1. Introduction

The determination of the effective moduli of composites has been widely investigated and several micromechanics approaches have been developed, which significantly improved the initial predictions. The dilute, self-consistent, differential and Mori–Tanaka methods are the micromechanics methods that have been extensively used, and they are all based on the two-phase model. The essential assumption in the dilute model is that a single inclusion is embedded in an infinite matrix subjected to a remote loading in the

* Corresponding author. Fax: +852-2559-5337.
E-mail address: hreccyk@hkucc.hku.hk (Y.K. Cheung).

0020-7683/03/$ - see front matter © 2002 Elsevier Science Ltd. All rights reserved.
doi:10.1016/S0020-7683(02)00606-6

Nomenclature

A_1, A_2, A_3 area of the fiber, matrix and composite in a three-phase model
L_1, L_2 the interface contour between the fiber, matrix and composite
u, v in-plane displacement components
F_x, F_y components of the in-plane stress resultants
OXY, Oxy global and local Cartesian coordinate systems
β angle made by the X-axis and x-axis
O_1, O_2 common foci of elliptical contours L_1 and L_2
$\sigma_{ij}, \varepsilon_{ij}$ stress and strain components
$B, G(G_T), E_L, G_{LT}, \nu_{LT}$ in-plane volume and shear moduli, longitudinal tensile and shear moduli, major Poisson's ratio of a transversely isotropic material
κ material constant, $\kappa = 3 - 4\nu$ for plane strain and $\kappa = (3 - \nu)/(1 + \nu)$ for plane stress, where ν is Poisson's ratio
λ fiber volume fraction
γ_1, γ_2 aspect ratio of elliptical contours L_1 and L_2
a_1, b_1, a_2, b_2 semimajor axes and semiminor axes of L_1 and L_2
z, ζ complex variable in physical plane and mapping plane
$\Omega(\zeta)$ mapping function
R a constant in the mapping function
A_1', A_2', A_3' image of A_1, A_2, A_3
L_0', L_1', L_2' image of O_1, O_2, L_1, L_2
ρ_0, ρ_1, ρ_2 radii of L_0', L_1', L_2'
ρ, θ polar coordinates in the ζ-plane
$\varphi^*(z), \psi^*(z)$ in-plane complex potentials in the physical plane (z-plane)
$\varphi(\zeta), \psi(\zeta)$ in-plane complex potentials in the mapping plane (ζ-plane)
$\Phi(\zeta), \Psi(\zeta), \omega(\zeta)$ defined by Eqs. (35) and (36)
$a_m, b_m, c_m, d_m, e_m, f_m$ coefficients of Laurent series
p_{ij}, q_{ij}, s_{ij} constants defined by Eq. (52)
J Jacobian
w antiplane displacement
$f(z)$ complex potential for antiplane strain
$\boldsymbol{M}_i$ moduli matrices
$\boldsymbol{A}$ strain gradient concentration matrix
$\mathbf{Z}_i$ strain vector
$\mathbf{Z}^\infty$ far-field strain vector
$\mathbf{Q}(\beta)$ transformation matrix
$\mathbf{I}$ third order unit matrix
$[\cdot]_{loc}$ subscript refers to the local Cartesian coordinates
$[\cdot]^{dil}, [\cdot]^{sc}, [\cdot]^{dif}, [\cdot]^{MT}$ superscripts refer to dilute approximation, self-consistent method, differential scheme and Mori–Tanaka method, respectively
$[\cdot]_a, [\cdot]_b, [\cdot]_c$ subscripts refer to the three fundamental problems defined by Eqs. (16)–(18), respectively
$[\cdot]_1, [\cdot]_2, [\cdot]_3$ subscripts refer to fiber, matrix and composite, respectively
$[\cdot]'$ superscript denotes the derivative with respect to the argument
$\bar{[\cdot]}$ above sign denotes averaging
$\bar{[\cdot]}$ above sign denotes complex conjugate

composites. The essential assumption in the self-consistent model is that a single inclusion is embedded in an infinite equivalent medium of the composites. Obviously, the dilute model ignores the inclusion interaction, while the self-consistent model overestimates it. The two models have traditionally received criticism on their accuracy. As an incremental form of the self-consistent method, the differential method does not exhibit the intuitively unacceptable results of the self-consistent method. However, it may lead to non-unique solutions (Norris, 1985). The key assumption in the Mori–Tanaka method is that a single inclusion is embedded in an infinite matrix subjected to an applied remote field equal to the as-yet-unknown average stress (strain) field in the matrix, and the method considerably improved the accuracy of the dilute method (Mori and Tanaka, 1973; Taya and Chou, 1981; Benveniste, 1985; Zhao and Weng, 1990). The pros and cons of the Mori–Tanaka method have been discussed by Christensen (1990) and Christensen et al. (1992).

The generalized self-consistent method is a more sophisticated micromechanics approach (Christensen and Lo, 1979; Luo and Weng, 1987; Christensen, 1993; Huang and Hu, 1995; Jiang and Cheung, 1998, 2001; Riccardi and Montheilet, 1999; Jiang et al., 2001). Different from the aforementioned micromechanics methods based on the two-phase model, the generalized self-consistent method is based on a three-phase model: an inclusion is embedded in a finite matrix, which in turn is embedded in an infinite composite with the as-yet-unknown effective moduli. The generalized self-consistent method provides accurate predictions for extreme types of inclusions (i.e. voids and rigid inclusions), and the method also gives the correct asymptotic behavior of composites as the inclusion volume fraction approaches 1 (fully packed). It is shown that the results of the generalized self-consistent method have excellent agreement with the experimental data (for example, refer to Huang et al., 1994). The three-phase model is also used to improve the accuracy of the Mori–Tanaka method (Luo and Weng, 1987).

However, most three-phase models can only accommodate cylindrical and spherical inclusions, and the studies are still insufficient on the generalized self-consistent method accounting for inclusion shape variations. Huang and Hu (1995) proposed a three-phase elliptical inclusion model where surrounding elliptical ring shares the same aspect ratio as the elliptical inclusion. They addressed the problem of an in-plane isotropic distribution of elliptical inclusions. Riccardi and Montheilet (1999) developed a generalized self-consistent method for solids containing randomly oriented spheroidal inclusions. Jiang and Cheung (1998) proposed a three-phase confocal elliptical cylinder model for fiber-reinforced composites. They addressed the problem of longitudinal shear, which is related to an effective modulus, i.e. the longitudinal shear modulus of fiber-reinforced composites.

The objective of this work is to develop a systematic generalized self-consistent method for fiber-reinforced composites based on the three-phase confocal elliptical cylinder model, so that all the five effective moduli can be reasonably predicted and the convergence of solutions can be guaranteed in various practical cases. Using the conformal mapping technique integrated with the Laurent series expansion, the analytical solutions for relevant plane strain, modified plane strain and longitudinal shear problems are derived. The algebraic equations are established for predicting all the five effective moduli of fiber-reinforced composites, accounting for the randomness in distribution and section orientation of fibers in a statistical sense. The dilute, self-consistent, Mori–Tanaka and differential methods are the micromechanics methods were first developed for monotonically aligned fiber-reinforced composites. In this paper the four micromechanics methods are also extended to cover the case of transversely randomly oriented fibers. (Note such an extension of the Mori–Tanaka method given by Zhao and Weng, 1990.) Thus a full comparison is made among various micromechanics methods and with Hashin and Shtrikman's upper and lower bounds (Hashin and Shtrikman, 1963).

Hu and Weng (2000a,b) shed light on the connections between several commonly used micromechanics models as well as the inclusion distribution functions in three-phase models. In this paper, the dependence of the distribution functions on the volume fraction is examined, and the reasonableness of the fiber distribution function in the three-phase confocal elliptical cylinder model is shown.

Finally the sensitivity of the five effective moduli to fiber shapes is examined. The study is useful in designing fiber-reinforced composites based on a fundamental understanding of the relation between the macroscopic properties and microstructures of composites.

2. Description of the plane strain problem

First, the plane strain problem of the three-phase confocal elliptical cylinder model is studied, which is related to the prediction of two effective moduli, i.e. the in-plane bulk and transverse shear moduli of fiber-reinforced composites. Fig. 1 is a schematic diagram of the model. The elliptical region A_1 encircled by the contour L_1 represents the fiber cross-section and the elliptical ring region A_2 between L_1 and L_2 represents the matrix in the representative unit cell. L_1 and L_2 share the common foci O_1 and O_2. The infinite region A_3 outside L_2 represents the equivalent medium of the composite with the as-yet-unknown effective elastic moduli, and the composite is transversely isotropic in a statistical sense. Building a local Cartesian coordinate system Oxy along the principal axes of the confocal ellipses, then the continuity conditions of the displacements and stresses on L_1 and L_2 can be expressed as

$$(u+\mathrm{i}v)_1 = (u+\mathrm{i}v)_2, \quad (F_x+\mathrm{i}F_y)_1 = (F_x+\mathrm{i}F_y)_2 \quad \text{on } L_1 \tag{1}$$

$$(u+\mathrm{i}v)_2 = (u+\mathrm{i}v)_3, \quad (F_x+\mathrm{i}F_y)_2 = (F_x+\mathrm{i}F_y)_3 \quad \text{on } L_2 \tag{2}$$

where u and v are the displacement components and F_x and F_y are the components of the stress resultants along any arc on L_1 or L_2; the subscripts 1, 2 and 3 refer to the fiber, matrix and equivalent medium of the composite in the three-phase model. Eqs. (1) and (2) have been cast in complex form for the convenience of analysis.

Letting OXY be the global Cartesian coordinate system and β be the angle made by the X-axis and x-axis (Fig. 1), we can write

$$\sigma_{XX} = \frac{\sigma_{yy}+\sigma_{xx}}{2} - \frac{\sigma_{yy}-\sigma_{xx}}{2}\cos 2\beta - \sigma_{xy}\sin 2\beta \tag{3}$$

$$\sigma_{YY} = \frac{\sigma_{yy}+\sigma_{xx}}{2} + \frac{\sigma_{yy}-\sigma_{xx}}{2}\cos 2\beta + \sigma_{xy}\sin 2\beta \tag{4}$$

$$\sigma_{XY} = -\frac{\sigma_{yy}-\sigma_{xx}}{2}\sin 2\beta + \sigma_{xy}\cos 2\beta \tag{5}$$

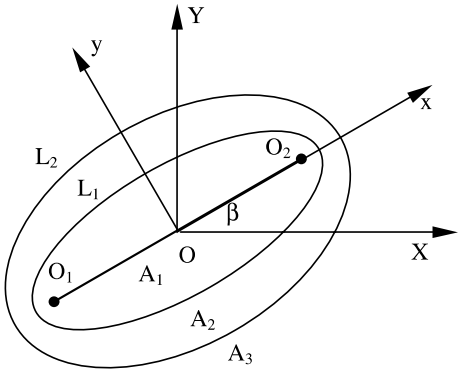

Fig. 1. Schematic diagram of the three-phase confocal elliptical cylinder model.

where $(\sigma_{XX}, \sigma_{YY}, \sigma_{XY})$ and $(\sigma_{xx}, \sigma_{yy}, \sigma_{xy})$ are the stress components in the global and local Cartesian coordinates, respectively.

The effective moduli of composites can be derived by considering the volume average of the stress and strain fields. Letting B_3 be the effective in-plane bulk modulus and G_3 be the effective transverse shear modulus, we have

$$\tilde{\sigma}_{XX} + \tilde{\sigma}_{YY} = 2B_3(\tilde{\varepsilon}_{XX} + \tilde{\varepsilon}_{YY}) \tag{6}$$

$$\tilde{\sigma}_{XY} = 2G_3\tilde{\varepsilon}_{XY} \tag{7}$$

where $\varepsilon_{XX}, \varepsilon_{YY}, \varepsilon_{XY}$ are the in-plane strain components in the global Cartesian coordinates; the above wave sign "$\sim$" denotes averaging.

According to the generalized self-consistent method, the volume fraction of the fiber in a representative unit cell (λ) is equal to that of the whole composite, so we have

$$\lambda = \frac{A_1}{A_1 + A_2} = \frac{a_1 b_1}{a_2 b_2} \tag{8}$$

where (a_1, b_1) and (a_2, b_2) are the semimajor axes and semiminor axes of L_1 and L_2, respectively. According to the generalized self-consistent method, Eqs. (6) and (7) hold for a representative unit cell. For the unit cell, the averaged stresses of the left-hand sides of the two equations can be expressed as

$$(\tilde{\sigma}_{XX} + \tilde{\sigma}_{YY}) = \lambda(\tilde{\sigma}_{XX} + \tilde{\sigma}_{YY})_1 + (1-\lambda)(\tilde{\sigma}_{XX} + \tilde{\sigma}_{YY})_2 \tag{9}$$

$$\tilde{\sigma}_{XY} = \lambda(\tilde{\sigma}_{XY})_1 + (1-\lambda)(\tilde{\sigma}_{XY})_2 \tag{10}$$

Analogous averaged strain expressions of the right-hand sides of Eqs. (6) and (7) can be arrived at. Thus, Eqs. (6) and (7) can be written as

$$\lambda(\tilde{\sigma}_{XX} + \tilde{\sigma}_{YY})_1 + (1-\lambda)(\tilde{\sigma}_{XX} + \tilde{\sigma}_{YY})_2 = B\left[\frac{\lambda}{B_1}(\tilde{\sigma}_{XX} + \tilde{\sigma}_{YY})_1 + \frac{(1-\lambda)}{B_2}(\tilde{\sigma}_{XX} + \tilde{\sigma}_{YY})_2\right] \tag{11}$$

$$\lambda(\tilde{\sigma}_{XY})_1 + (1-\lambda)(\tilde{\sigma}_{XY})_2 = G\left[\frac{\lambda}{G_1}(\tilde{\sigma}_{XY})_1 + \frac{(1-\lambda)}{G_2}(\tilde{\sigma}_{XY})_2\right] \tag{12}$$

Obviously, the key work is to determine the averaged stress fields. Averaging of the stress fields should be taken over the region under consideration, as well as over the orientation β, which is based on the assumption of statistical uniformity.

$$\tilde{\sigma}_{IJ} = \frac{1}{2\pi A}\int_0^{2\pi}\int_A \sigma_{IJ}\,\mathrm{d}A\,\mathrm{d}\beta \quad I,J = X,Y \tag{13}$$

where A is the area. For brevity, the conventional indicial notation of the stress is used.

It is seen from Eqs. (11) and (12) that two kinds of remote uniform stress state in the global coordinates should be considered to determine the two effective moduli B_3 and G_3:

(1) Remote biaxial tension

$$\sigma^{\infty}_{XX} = \sigma^{\infty}_{YY} \neq 0, \quad \sigma^{\infty}_{XY} = 0 \tag{14}$$

(2) Remote shear

$$\sigma^{\infty}_{XX} = \sigma^{\infty}_{YY} = 0, \quad \sigma^{\infty}_{XY} \neq 0 \tag{15}$$

Substituting Eqs. (3)–(5) into Eq. (13), it is seen that the double integral is uncoupled and the integral over the orientation β can be completed in closed form. Thus, the work boils down to obtaining the stress field of the following three fundamental problems in the local coordinate system (also consult Huang and Hu, 1995):

(a) Remote unit biaxial tension

$$\sigma_{xx}^{\infty} = \sigma_{yy}^{\infty} = 1, \quad \sigma_{xy}^{\infty} = 0 \tag{16}$$

In this case, the normal stresses are denoted by σ_{xxa} and σ_{yya}.

(b) Remote unit biaxial tension/compression

$$\sigma_{xx}^{\infty} = -\sigma_{yy}^{\infty} = -1, \quad \sigma_{xy}^{\infty} = 0 \tag{17}$$

In this case, the normal stresses are denoted by σ_{xxb} and σ_{yyb}.

(c) Remote unit shear

$$\sigma_{xx}^{\infty} = \sigma_{yy}^{\infty} = 0, \quad \sigma_{xy}^{\infty} = 1 \tag{18}$$

In this case, the shear stress is denoted by σ_{xyc}.

Once the solutions to the three fundamental problems are available, the averaged stresses in Eqs. (11) and (12) (in the global coordinate system) can be obtained from the following equations:

$$(\tilde{\sigma}_{XX} + \tilde{\sigma}_{YY})_k = (\tilde{\sigma}_{xxa} + \tilde{\sigma}_{yya})_k \sigma_{XX}^{\infty} \tag{19}$$

$$(\tilde{\sigma}_{XY})_k = \left[\frac{1}{4}(\tilde{\sigma}_{yyb} - \tilde{\sigma}_{xxb})_k + \frac{1}{2}(\tilde{\sigma}_{xyc})_k\right]\sigma_{XY}^{\infty} \tag{20}$$

where the subscript $k = 1, 2$ refers to the fiber and matrix in a representative unit cell, and averaging of the stresses for the three basic problems is taken only over the regions under consideration. (The orientation averaging in a statistical sense has been finished.)

3. Complex potentials solutions of the fundamental problems

In formulating the fundamental problems, we use the two complex potentials $\varphi^*(z)$ and $\psi^*(z)$ (two analytical functions, $z = x + \mathrm{i}y$) of Muskhelishivili (1975). The stress components $(\sigma_{xx}, \sigma_{yy}, \sigma_{xy})$, the displacement components (u, v) and the components of the resultant stress (F_x, F_y) in Cartesian coordinates are related to $\varphi^*(z)$ and $\psi^*(z)$ such that

$$\sigma_{xx} + \sigma_{yy} = 2\lfloor \varphi^{*\prime}(z) + \overline{\varphi^{*\prime}(z)} \rfloor \tag{21}$$

$$\sigma_{yy} - \sigma_{xx} + 2\mathrm{i}\sigma_{xy} = 2\left[\bar{z}\varphi^{*\prime\prime}(z) + \psi^{*\prime}(z)\right] \tag{22}$$

$$2G(u + \mathrm{i}v) = \kappa\varphi^*(z) - z\overline{\varphi^{*\prime}(z)} - \overline{\psi^*(z)} \tag{23}$$

$$(F_x + \mathrm{i}F_y) = -\mathrm{i}\left[\varphi^*(z) + z\overline{\varphi^{*\prime}(z)} + \overline{\psi^*(z)}\right]_A^B \tag{24}$$

where $\kappa = 3 - 4\nu$ for plane strain and $\kappa = (3 - \nu)/(1 + \nu)$ for plane stress, G and ν are shear modulus and Poisson's ratio, respectively; the overbar represents the complex conjugate, the prime denotes differentiation

with respect to the argument and $[\cdot]_A^B$ signifies the change in the bracketed function in moving from point A to point B along any arc AB.

To solve the problem, another complex variable

$$\zeta = \xi + \mathrm{i}\eta = \rho\,\mathrm{e}^{\mathrm{i}\theta} \tag{25}$$

is introduced, where ρ and θ are the polar coordinates in the complex ζ-plane. Making use of the conformal transformation of the z-plane onto the ζ-plane (Muskhelishivili, 1975)

$$z = \Omega(\zeta) = R\left(\zeta + \frac{1}{\zeta}\right) \tag{26}$$

where R is a constant to be determined, the regions A_1, A_2 and A_3 (infinite region) divided by the imaginary cut O_1O_2, the elliptical contours L_1, L_2 in the z-plane (Oxy-plane, Fig. 1) are mapped onto the circular ring regions A_1', A_2' and A_3' divided by L_0', L_1' and L_2' with radii $\rho_0 = 1$, ρ_1 and ρ_2 in the ζ-plane (Fig. 2), respectively.

From this transformation, it is seen that

$$x = R\left(\rho + \frac{1}{\rho}\right)\cos\theta, \quad y = R\left(\rho - \frac{1}{\rho}\right)\sin\theta \tag{27}$$

$$a_k = R\left(\rho_k + \frac{1}{\rho_k}\right), \quad b_k = R\left(\rho_k - \frac{1}{\rho_k}\right) \qquad k = 1, 2 \tag{28}$$

Since the geometrical parameters of the fiber section, a_1 and b_1, are known, R and ρ_1 can be determined by using Eq. (28). The substitution of Eq. (28) into Eq. (8) yields

$$\lambda = \frac{\rho_1^2 - 1/\rho_1^2}{\rho_2^2 - 1/\rho_2^2} \tag{29}$$

in terms of which, ρ_2 can be determined as the volume fraction of fibers, λ, is prescribed.

With the aid of Eq. (26), Eqs. (21)–(24) can be written as

$$\sigma_x + \sigma_y = 2\lfloor \Phi(\zeta) + \overline{\Phi(\zeta)} \rfloor \tag{30}$$

$$\sigma_{yy} - \sigma_{xx} + 2\mathrm{i}\sigma_{xy} = 2\left[\frac{\overline{\Omega(\zeta)}}{\Omega'(\zeta)}\Phi'(\zeta) + \Psi(\zeta)\right] \tag{31}$$

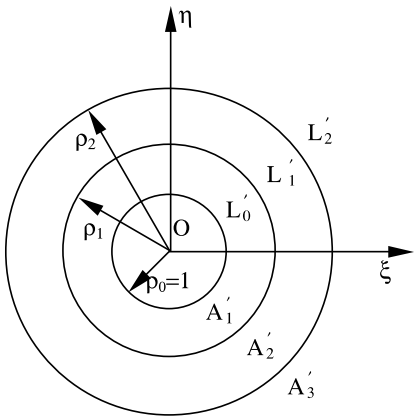

Fig. 2. Conformal mapping.

$$2G(u+\mathrm{i}v)=\kappa\varphi(\zeta)-\Omega(\zeta)\overline{\Phi(\zeta)}-\overline{\psi(\zeta)} \tag{32}$$

$$F_x+\mathrm{i}F_y=-\mathrm{i}\left[\varphi(\zeta)+\Omega(\zeta)\overline{\Phi(\zeta)}+\overline{\psi(\zeta)}\right]_A^B \tag{33}$$

where

$$\varphi(\zeta)=\varphi^*[\Omega(\zeta)],\quad \psi(\zeta)=\psi^*[\Omega(\zeta)] \tag{34}$$

$$\Phi(\zeta)=\varphi'(\zeta)/\Omega'(\zeta),\quad \Psi(\zeta)=\psi'(\zeta)/\Omega'(\zeta) \tag{35}$$

Letting

$$\omega(\zeta)=\bar{z}\varphi^{*\prime}(z)+\psi^*(z)=\frac{\overline{\Omega(\zeta)}}{\Omega'(\zeta)}\varphi'(\zeta)+\psi(\zeta) \tag{36}$$

and substituting Eqs. (32) and (33) into Eqs. (1) and (2), the continuity conditions of the displacements and stresses on L_1 and L_2 are expressed as

$$\frac{1}{G_1}[\kappa_1\varphi_1(\zeta)-\overline{\omega_1(\zeta)}]=\frac{1}{G_2}[\kappa_2\varphi_2(\zeta)-\overline{\omega_2(\zeta)}]\quad \zeta=\rho_1\mathrm{e}^{\mathrm{i}\theta} \tag{37}$$

$$\varphi_1(\zeta)+\overline{\omega_1(\zeta)}=\varphi_2(\zeta)+\overline{\omega_2(\zeta)}\quad \zeta=\rho_1\mathrm{e}^{\mathrm{i}\theta} \tag{38}$$

$$\frac{1}{G_2}[\kappa_2\varphi_2(\zeta)-\overline{\omega_2(\zeta)}]=\frac{1}{G_3}[\kappa_3\varphi_3(\zeta)-\overline{\omega_3(\zeta)}]\quad \zeta=\rho_2\mathrm{e}^{\mathrm{i}\theta} \tag{39}$$

$$\varphi_2(\zeta)+\overline{\omega_2(\zeta)}=\varphi_3(\zeta)+\overline{\omega_3(\zeta)}\quad \zeta=\rho_2\mathrm{e}^{\mathrm{i}\theta} \tag{40}$$

where subscripts 1, 2 and 3 refer to the media in regions A_1, A_2 and A_3, respectively. It is important to note that $\omega(\zeta)$ is not an analytical function and its series expansion should be derived by Eq. (36) based on the Laurent expansions of $\varphi(\zeta)$ and $\psi(\zeta)$. First, we consider the symmetrical fundamental problems (a) and (b). The analytical functions $\varphi_k(\zeta)$ and $\psi_k(\zeta)$ $(k=1,2,3)$ can be expanded into Laurent series

$$\varphi_1(\zeta)=\sum_{m=1,3}^{\infty}a_m(\zeta^m+\zeta^{-m}),\quad \psi_1(\zeta)=\sum_{m=1,3}^{\infty}b_m(\zeta^m+\zeta^{-m}) \tag{41}$$

$$\varphi_2(\zeta)=\sum_{m=1,3}^{\infty}(c_m\zeta^m+c_{-m}\zeta^{-m}),\quad (1-\zeta^{-2})\psi_2(\zeta)=\sum_{m=1,3}^{\infty}(d_m\zeta^m+d_{-m}\zeta^{-m}) \tag{42}$$

$$\varphi_3(\zeta)=e_1\zeta+\sum_{m=1,3}^{\infty}e_{-m}\zeta^{-m},\quad (1-\zeta^{-2})\psi_3(\zeta)=\left(f_1\zeta+\sum_{m=1,3}^{\infty}f_{-m}\zeta^{-m}\right) \tag{43}$$

where each expansion contains only odd terms, and a_m, b_m, c_m, c_{-m}, d_m, d_{-m}, e_{-m}, f_{-m}, e_1, f_1 are real constants by the consideration of symmetry. An observation upon Eqs. (36)–(40) and the numerical computations shows that it is more efficient to use the Laurent expansions of $(1-\zeta^{-2})\psi_2(\zeta)$ and $(1-\zeta^{-2})\psi_3(\zeta)$ instead of those of $\psi_2(\zeta)$ and $\psi_3(\zeta)$, respectively. Since O_1O_2 is only an imaginary cut and $\varphi_1(\zeta)$ and $\psi_1(\zeta)$ should be holomorphic in the region A_1, such that

$$\varphi_1(\mathrm{e}^{\mathrm{i}\theta})=\varphi_1(\mathrm{e}^{-\mathrm{i}\theta}),\quad \psi_1(\mathrm{e}^{\mathrm{i}\theta})=\psi_1(\mathrm{e}^{-\mathrm{i}\theta}) \tag{44}$$

which leads to $a_{-m}=a_m$, $b_{-m}=b_m$. Besides the bounded stresses at infinity lead to $e_m=f_m=0$ as $m\geqslant 2$.

By using the remote field conditions (16) and (17), we obtain

$$e_1 = \frac{1}{2}, \quad f_1 = 0 \tag{45}$$

for the fundamental problem (a) and

$$e_1 = 0, \quad f_1 = 1 \tag{46}$$

for the fundamental problem (b).

$\varphi_k(\zeta)$ and $\psi_k(\zeta)$ $(k = 1, 2, 3)$ for the antisymmetrical fundamental problem (c) have the same Laurent expansions except that the unknown constants a_m, b_m, c_m, c_{-m}, d_m, d_{-m}, e_{-m}, f_{-m}, e_1, f_1 in Eqs. (41)–(43) are replaced by $\mathrm{i}a_m$, $\mathrm{i}b_m$, $\mathrm{i}c_m$, $\mathrm{i}c_{-m}$, $\mathrm{i}d_m$, $\mathrm{i}d_{-m}$, $\mathrm{i}e_{-m}$, $\mathrm{i}f_{-m}$, $\mathrm{i}e_1$, $\mathrm{i}f_1$. By using the remote field conditions (18), we obtain

$$e_1 = 0, \quad f_1 = 1 \tag{47}$$

Letting the expansions of $\varphi_k(\zeta)$ and $\psi_k(\zeta)$ $(k = 1, 2, 3)$ are truncated at $m = 2M - 1$, there are $8M$ unknown constants to be determined. After some arrangement, the continuity conditions (37)–(40) can be written as

$$p_{12}\overline{\varphi_1(\zeta)} - s_{12}\omega_1(\zeta) - p_{22}\overline{\varphi_2(\zeta)} = 0 \quad \zeta = \rho_1 \mathrm{e}^{\mathrm{i}\theta} \tag{48}$$

$$(1 - \zeta^{-2})\lfloor q_{21}\overline{\varphi_1(\zeta)} + p_{21}\omega_1(\zeta) - p_{22}\omega_2(\zeta)\rfloor = 0 \quad \zeta = \rho_1 \mathrm{e}^{\mathrm{i}\theta} \tag{49}$$

$$(1 - \zeta^{-2})\lfloor p_{23}\overline{\varphi_2(\zeta)} - s_{23}\omega_2(\zeta) - p_{33}\overline{\varphi_3(\zeta)}\rfloor = 0 \quad \zeta = \rho_2 \mathrm{e}^{\mathrm{i}\theta} \tag{50}$$

$$(1 - \zeta^{-2})\lfloor q_{32}\overline{\varphi_2(\zeta)} + p_{32}\omega_2(\zeta) - p_{33}\omega_3(\zeta)\rfloor = 0 \quad \zeta = \rho_2 \mathrm{e}^{\mathrm{i}\theta} \tag{51}$$

where

$$p_{ij} = \frac{\kappa_i}{G_i} + \frac{1}{G_j}, \quad q_{ij} = \pm\left(\frac{\kappa_i}{G_i} - \frac{\kappa_j}{G_j}\right), \quad s_{ij} = \pm\left(\frac{1}{G_i} - \frac{1}{G_j}\right) \tag{52}$$

where q_{ij} and s_{ij} have sign (+) for the symmetrical fundamental problems (a) and (b), and sign (−) for the antisymmetrical fundamental problem (c), respectively.

Substituting the expansions (41)–(43) truncated at $m = 2M - 1$ into Eqs. (48)–(51), we obtain $8M$ linear algebraic equations with respect to the $8M$ unknown constants. It is seen that e_{-m} and f_{-m} $(m = 1, 3, \ldots, 2M - 1)$ are easy to be expressed by the other unknown coefficients. Finally, we can obtain $6M$ equations to determine the remaining $6M$ unknown coefficients, and the equations are listed in Appendix A. Now the three fundamental problems have been formulated.

4. Prediction of the effective transverse moduli

To predict the effective transverse moduli of fiber-reinforced composites by using Eqs. (11) and (12), we must derive the detailed expression of the averaged stresses. Substituting Eqs. (41)–(43) into Eqs. (30) and (31), then averaging over the corresponding regions, we can find that the averaged stresses in the three fundamental problems are only related to some coefficients of the expansions of $\varphi_k(\zeta)$ and $\psi_k(\zeta)$ $(k = 1, 2, 3)$:

$$(\tilde{\sigma}_{xxa} + \tilde{\sigma}_{yya})_1 = \frac{4}{A_1}\iint_{A_1} \mathrm{Re}[\Phi_1^*(z)]\,\mathrm{d}A_1 = \frac{4}{A_1}\iint_{A_1'} \mathrm{Re}[\Phi_1(\zeta)]J\,\mathrm{d}A_1' = 4(a_1)_{\mathrm{a}} \tag{53}$$

$$(\tilde{\sigma}_{xxa}+\tilde{\sigma}_{yya})_2=\frac{4}{A_2}\iint_{A_2'}\mathrm{Re}[\Phi_2(\zeta)]J\,\mathrm{d}A_2'=4\left(\frac{c_1+\frac{c_{-1}}{\rho_1^2\rho_2^2}}{1+\frac{1}{\rho_1^2\rho_2^2}}\right)_{\mathrm{a}} \tag{54}$$

$$(\tilde{\sigma}_{yyb}-\tilde{\sigma}_{xxb})_1=\frac{2}{A_1}\iint_{A_1'}\mathrm{Re}\left[\frac{\overline{\Omega(\zeta)}}{\Omega'(\zeta)}\Phi_1'(\zeta)+\Psi_1(\zeta)\right]J\,\mathrm{d}A_1'=2\left[b_1+\left(\rho_1^2+\frac{1}{\rho_1^2}\right)\sum_{m=3,5}^{\infty}ma_m\right]_{\mathrm{b}} \tag{55}$$

$$\begin{aligned}(\tilde{\sigma}_{yyb}-\tilde{\sigma}_{xxb})_2&=\frac{2}{A_2}\iint_{A_2'}\mathrm{Re}\left[\frac{\overline{\Omega(\zeta)}}{\Omega'(\zeta)}\Phi_2'(\zeta)+\Psi_2(\zeta)\right]J\,\mathrm{d}A_2'\\&=\left(\frac{2}{1+\frac{1}{\rho_1^2\rho_2^2}}\right)\left[d_1+\frac{d_1+d_{-1}}{\rho_1^2\rho_2^2}+\frac{(\rho_1^2+\rho_2^2)(c_1-c_{-1})}{\rho_1^4\rho_2^4}+\left(1+\frac{1}{\rho_1^4\rho_2^4}\right)\sum_{m=3,5}^{\infty}mc_m\right]_{\mathrm{b}}\end{aligned} \tag{56}$$

$$(\tilde{\sigma}_{xye})_1=\frac{1}{A_1}\iint_{A_1'}\mathrm{Im}\left[\frac{\overline{\Omega(\zeta)}}{\Omega'(\zeta)}\Phi_1'(\zeta)+\Psi_1(\zeta)\right]J\,\mathrm{d}A_1'=\left[b_1+\left(\rho_1^2+\frac{1}{\rho_1^2}\right)\sum_{m=3,5}^{\infty}ma_m\right]_{\mathrm{c}} \tag{57}$$

$$\begin{aligned}(\tilde{\sigma}_{xye})_2&=\frac{1}{A_2}\iint_{A_2'}\mathrm{Im}\left[\frac{\overline{\Omega(\zeta)}}{\Omega'(\zeta)}\Phi_2'(\zeta)+\Psi_2(\zeta)\right]J\,\mathrm{d}A_2'\\&=\left(\frac{1}{1+\frac{1}{\rho_1^2\rho_2^2}}\right)\left[d_1+\frac{d_1+d_{-1}}{\rho_1^2\rho_2^2}+\frac{(\rho_1^2+\rho_2^2)(c_1-c_{-1})}{\rho_1^4\rho_2^4}+\left(1+\frac{1}{\rho_1^4\rho_2^4}\right)\sum_{m=3,5}^{\infty}mc_m\right]_{\mathrm{c}}\end{aligned} \tag{58}$$

where the subscripts a, b and c refer to the three fundamental problems; J is the Jacobian:

$$J=\rho+\frac{1}{\rho^3}-\frac{2}{\rho}\cos 2\theta \tag{59}$$

Substituting Eqs. (53)–(58) into Eqs. (19) and (20), then into Eqs. (11) and (12), we obtain two equations to determine the effective moduli B_3 and G_3. It is noted that B_i is related to κ_i:

$$B_i=\frac{2G_i}{\kappa_i-1},\quad i=1,2,3 \tag{60}$$

Since the coefficients of the complex potentials expansions contain the as-yet-unknown moduli B_3 and G_3, the two equations are implicit ones, which must be solved simultaneously with Eqs. (A.1)–(A.6). Taking Voigt approximation as the initial value of iteration, the equations converge rapidly and steadily. Voigt approximation is as follows:

$$B_3=\lambda B_1+(1-\lambda)B_2 \tag{61}$$

$$G_3=\lambda G_1+(1-\lambda)G_2 \tag{62}$$

5. Prediction of the longitudinal tension and shear moduli, and major Poisson's ratio

The method developed in the preceding sections can be extended to estimate the effective longitudinal tension modulus E_{L3}, major Poisson's ratio v_{LT3} and longitudinal shear modulus G_{LT3} of fiber-reinforced composites, which will be briefly described in this section.

The effective longitudinal tension modulus E_{L3} and major Poisson's ratio v_{LT3} can be predicted by considering a "modified plane strain" problem. We assume that a longitudinal (axial) force is applied to the three-phase confocal elliptical cylinder model so that the longitudinal strain of the model is a constant $\varepsilon_{ZZ}^{\infty}$. If various phases of the model are not restrained, the transverse strains should be

$$\varepsilon_{XX1} = -v_{LT1}\varepsilon_{ZZ}^{\infty}, \quad \varepsilon_{XX2} = -v_{LT2}\varepsilon_{ZZ}^{\infty}, \quad \varepsilon_{XX3} = -v_{LT3}\varepsilon_{ZZ}^{\infty} \tag{63}$$

where subscripts 1, 2 and 3 refer to the fiber, matrix and composite, respectively. In this imaginary case, the in-plane (transverse) displacements of the separate phases can be written as

$$(u + \mathrm{i}v)_{10} = -v_{LT1}\varepsilon_{ZZ}^{\infty} z, \quad (u + \mathrm{i}v)_{20} = -v_{LT2}\varepsilon_{ZZ}^{\infty} z, \quad (u + \mathrm{i}v)_{30} = -v_{LT3}\varepsilon_{ZZ}^{\infty} z \tag{64}$$

where they are cast into complex form for the convenience of analysis, and $z = x + \mathrm{i}y$.

When the separate phases are combined together, a mismatch of the displacements occurs, which leads to the internal boundary conditions of in-plane stresses and displacements on the interfaces L_1 and L_2 (refer to Fig. 1):

$$(u + \mathrm{i}v)_1 = (u + \mathrm{i}v)_2 - (v_{LT2} - v_{LT1})\varepsilon_{ZZ}^{\infty} z, \quad (F_x + \mathrm{i}F_y)_1 = (F_x + \mathrm{i}F_y)_2 \quad \text{on } L_1 \tag{65}$$

$$(u + \mathrm{i}v)_2 = (u + \mathrm{i}v)_3 - (v_{LT3} - v_{LT2})\varepsilon_{ZZ}^{\infty} z, \quad (F_x + \mathrm{i}F_y)_2 = (F_x + \mathrm{i}F_y)_3 \quad \text{on } L_2 \tag{66}$$

In this case the in-plane stress at infinity should vanish, so we have the remote field conditions

$$\sigma_{XX}^{\infty} = \sigma_{YY}^{\infty} = \sigma_{XY}^{\infty} = 0 \tag{67}$$

The modified in-plane problem produced by the longitudinal force can be solved by a similar method given in the preceding sections. To give the prediction of the effective longitudinal modulus E_{L3} and major Poisson's ratio v_{LT3}, two additional equations are required. Considering the relation of stresses and strains in the representative unit cell and averaging over the fiber section orientation, we can obtain two additional equations:

$$E_{L3} = \lambda E_{L1} + (1-\lambda)E_{L2} + \lambda v_{LT1}\frac{(\tilde{\sigma}_{XX} + \tilde{\sigma}_{YY})_1}{\varepsilon_{ZZ}^{\infty}} + (1-\lambda)v_{LT2}\frac{(\tilde{\sigma}_{XX} + \tilde{\sigma}_{YY})_2}{\varepsilon_{ZZ}^{\infty}} \tag{68}$$

$$v_{LT3} = \lambda v_{LT1} + (1-\lambda)v_{LT2} - \lambda\frac{(\tilde{\sigma}_{XX} + \tilde{\sigma}_{YY})_1}{4B_1\varepsilon_{ZZ}^{\infty}} - (1-\lambda)\frac{(\tilde{\sigma}_{XX} + \tilde{\sigma}_{YY})_2}{4B_2\varepsilon_{ZZ}^{\infty}} \tag{69}$$

The effective longitudinal shear modulus G_{LT3} of fiber-reinforced composites can be predicted by considering a remote antiplane loading. The antiplane displacement w, antiplane shear stress components σ_{xz} and σ_{yz} can be expressed by an analytical function $f(z)$:

$$w = \mathrm{Re}[f(z)] \tag{70}$$

$$\sigma_{xz} - \mathrm{i}\sigma_{yz} = G_{LT}f'(z) \tag{71}$$

This is a simpler problem than the in-plane problem. Similarly, the problem can be solved by using the conformal mapping technique integrated with the Laurent series expansion technique and the detail refers to Jiang and Cheung (1998).

6. Fiber distribution function

Recently, Hu and Weng (2000a,b) shed light on connections between several commonly used micromechanics models as well as the inclusion distribution functions in three-phase models. In the three-dimension case, the inclusions are taken to be ellipsoidal, and the spatial distribution of inclusions is also

taken to be ellipsoidal. The distribution ellipsoid is defined from the conditional probability density function that an inclusion centered at one point given that there is an inclusion centered at another point.

The outer elliptical contour L_2 (Fig. 1) of the three-phase confocal elliptical cylinder model (two-dimension problem) represents also the fiber distribution function. An important problem is whether the shape of the distribution ellipse depends on the fiber volume fraction λ while holding the fiber section aspect ratio ($\gamma_1 = b_1/a_1$) fixed.

To answer this problem, consider two extreme cases. One is the case of $\lambda \to 0$. As shown in Fig. 3a, at a very low volume fraction of fibers, the fiber section shape has little influence on the distribution function of fibers. For an isotropic fiber distribution in a statistical sense, the distribution function can be defined by a circle, or more exactly, by an ellipse of $\gamma_2 = b_2/a_2 \to 1$, where a_2 and b_2 are the semimajor and semiminor axes of the outer elliptical contour L_2. However, at a relatively high volume fraction of fibers, the distribution circle may fail to enclose completely the fiber (section) as shown in Fig. 3b. As a consequence, the predictions for effective moduli may fall outside the Hashin–Shtrikman's bounds (refer to Hu and Weng, 2000a,b). Apparently, in this case, the distribution function defined by a circle is improper, instead, a distribution ellipse should be taken. Further examine the extreme case of $\lambda \to 1$. As shown in Fig. 3c, in this case, the interphase (matrix) of the three-phase model becomes very small, so L_2 approaches to L_1, and $\gamma_2 \to \gamma_1$. It is concluded that the aspect ratio γ_2 of the distribution ellipse does depend on the fiber volume fraction λ while holding the fiber section aspect ratio γ_1 fixed, and γ_2 varies from 1 to γ_1 as λ goes up from 0 to 1.

Go back to the three-phase confocal elliptical model. From Eq. (28), it is seen that

$$\gamma_k = \frac{b_k}{a_k} = \frac{\rho_k^2 - 1}{\rho_k^2 + 1}, \quad k = 1, 2 \tag{72}$$

then from Eq. (29) and (72), it follows

$$\gamma_2 = \frac{(\gamma_1^2 - 1)\lambda + \sqrt{(\gamma_1^2 - 1)^2\lambda^2 + 4\gamma_1^2}}{2\gamma_1} \tag{73}$$

The variations of γ_2 with λ are depicted in Fig. 4 for several given values of γ_1. It is seen that γ_2 varies from 1 to γ_1 as λ goes up from 0 to 1. Eq. (73) and Fig. 4 indicate that the three-phase confocal elliptical model reasonably reflects the dependence of the distribution function of fibers on the volume fraction of fibers.

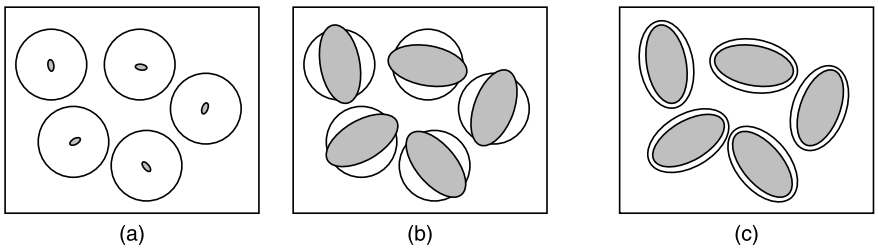

Fig. 3. The distribution function of fibers: (a) circular distribution at a very low volume fraction; (b) circular distribution at a relatively high volume fraction; (c) elliptical distribution at a very high volume fraction.

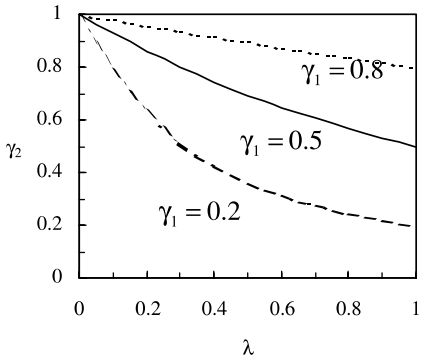

Fig. 4. Variations of the aspect ratio γ_2 of the distribution ellipse with the fiber volume fraction λ for several given values γ_1 of the fiber aspect ratio.

7. Other micromechanics methods

It is of interest to make a full comparison among various micromechanics predictions and with Hashin and Shtrikman's upper and lower bounds. The other micromechanics methods that have received the most attention and used are the dilute, self-consistent, Mori–Tanaka and differential methods. These methods have been developed for monotonically aligned fiber-reinforced composites. In this section, they will be extended to cover the case with transversely randomly oriented elliptical fibers. (Note such an extension of the Mori–Tanaka method given by Zhao and Weng, 1990.)

In formulating the micromechanics theories, it is convenient to adopt matrix notations, which are denoted by bold letters. The matrix equation for predicting the effective moduli of two-phase perfectly bonded fiber-reinforced composites can be written as (for example, refer to Dunn and Taya, 1993)

$$\mathbf{M}_3 = \mathbf{M}_2 + \lambda(\mathbf{M}_1 - \mathbf{M}_2)\mathbf{A} \tag{74}$$

where $\mathbf{M}_1$, $\mathbf{M}_2$ and $\mathbf{M}_3$ denote the moduli matrices of the fiber, matrix and composite, respectively. $\mathbf{A}$ is the strain gradient concentration matrix, which relates the averaged strain gradient in the inclusion (fiber) phase to that in the composite, i.e.

$$\widetilde{\mathbf{Z}}_1 = \mathbf{A}\widetilde{\mathbf{Z}}_3 = \mathbf{A}\mathbf{Z}^{\infty} \tag{75}$$

where $\mathbf{Z}^{\infty}$ is the homogeneous far-field strain; $\widetilde{\mathbf{Z}}_1$ and $\widetilde{\mathbf{Z}}_3$ are the averaged strain of the fiber and composite, respectively. For plane strain

$$\mathbf{Z} = [\,\varepsilon_{xx} \quad \varepsilon_{yy} \quad \varepsilon_{xy}\,]^{\mathrm{T}} \tag{76}$$

Let a composite with monotonically aligned fibers be subjected to homogeneous displacement boundary conditions. Then the averaged strain of fibers in the local Cartesian coordinates (Fig. 1) can be expressed as

$$(\widetilde{\mathbf{Z}}_1)_{\mathrm{loc}} = \mathbf{A}_{\mathrm{loc}}(\mathbf{Z}^{\infty})_{\mathrm{loc}} = \mathbf{A}_{\mathrm{loc}}\mathbf{Q}(\beta)\mathbf{Z}^{\infty} \tag{77}$$

where the subscript loc refers to the local Cartesian coordinates, so that $\mathbf{A}_{\mathrm{loc}}$, $(\widetilde{\mathbf{Z}}_1)_{\mathrm{loc}}$ and $(\mathbf{Z}^{\infty})_{\mathrm{loc}}$ are the strain gradient concentration, averaged fiber strain and far-field strain matrices in the local coordinates, respectively; $\mathbf{Q}(\beta)$ is the transformation matrix from the global coordinate system to the local coordinate system. For plane strain, $\mathbf{Q}(\beta)$ is a third order matrix:

$$\mathbf{Q}(\beta)=\begin{bmatrix}\cos^2\beta & \sin^2\beta & \sin 2\beta\\ \sin^2\beta & \cos^2\beta & -\sin 2\beta\\ -\frac{\sin 2\beta}{2} & \frac{\sin 2\beta}{2} & \cos 2\beta\end{bmatrix} \tag{78}$$

Consider the randomness of fiber section orientation in a statistical sense. Averaging of the fiber strain over the orientation β in the global coordinate system yields

$$\widetilde{\mathbf{Z}}_1=\frac{1}{\pi}\int_0^{\pi}\mathbf{Q}(-\beta)(\widetilde{\mathbf{Z}}_1)_{\mathrm{loc}}\,\mathrm{d}\beta=\left(\frac{1}{\pi}\int_0^{\pi}\mathbf{Q}(-\beta)\mathbf{A}_{\mathrm{loc}}\mathbf{Q}(\beta)\,\mathrm{d}\beta\right)\mathbf{Z}^{\infty} \tag{79}$$

A comparison between Eqs. (75) and (79) results in the strain gradient concentration matrix $\mathbf{A}$ in the global coordinate system in a statistical sense:

$$\mathbf{A}=\frac{1}{\pi}\int_0^{\pi}\mathbf{Q}(-\beta)\mathbf{A}_{\mathrm{loc}}\mathbf{Q}(\beta)\,\mathrm{d}\beta \tag{80}$$

It is seen that different micromechanics models may result in different approximations of $\mathbf{A}_{\mathrm{loc}}$:

(1) *Dilute approximation*. The key assumption made in the dilute approximation is that the interaction among inclusions in the matrix-based composite can be ignored. The strain gradient concentration matrix in the local coordinates can be expressed as (for example, see Dunn and Taya, 1993)

$$\mathbf{A}_{\mathrm{loc}}^{\mathrm{dil}}=[\mathbf{I}+\mathbf{S}_2\mathbf{M}_2^{-1}(\mathbf{M}_1-\mathbf{M}_2)]^{-1} \tag{81}$$

where the superscript dil signifies the dilute approximation, $\mathbf{I}$ is the third order unit matrix, $\mathbf{S}_2$ is the matrix representation of Eshelby's tensor (Eshelby, 1957). In the case of an infinite matrix containing an elliptical cylinder inclusion,

$$\mathbf{S}_2=\frac{1}{2(1-v_2)}\begin{bmatrix}\gamma_1\left(\frac{2+\gamma_1}{(1+\gamma_1)^2}+\frac{1-2v_2}{1+\gamma_1}\right) & \gamma_1\left(\frac{\gamma_1}{(1+\gamma_1)^2}-\frac{1-2v_2}{1+\gamma_1}\right) & 0\\ \left(\frac{1}{(1+\gamma_1)^2}-\frac{1-2v_2}{1+\gamma_1}\right) & \left(\frac{1+2\gamma_1}{(1+\gamma_1)^2}+\frac{1-2v_2}{1+\gamma_1}\right) & 0\\ 0 & 0 & \left(\frac{1+\gamma_1^2}{(1+\gamma_1)^2}+1-2v_2\right)\end{bmatrix} \tag{82}$$

where v_2 is Poisson's ratio of matrix material and γ_1 is the aspect ratio of inclusion section.

(2) *Self-consistent method*. The essential assumption employed in the self-consistent method is that each inclusion (fiber) is embedded in the equivalent medium with as-yet-unknown moduli. In this case

$$\mathbf{A}_{\mathrm{loc}}^{\mathrm{sc}}=[\mathbf{I}+\mathbf{S}_3\mathbf{M}_3^{-1}(\mathbf{M}_1-\mathbf{M}_3)]^{-1} \tag{83}$$

It is seen that Eq. (83) is arrived at by replacing $\mathbf{S}_2$ and $\mathbf{M}_2$ for the matrix in Eq. (81) with $\mathbf{S}_3$ and $\mathbf{M}_3$ for the composite.

(3) *Differential scheme*. The differential scheme can be regarded as an incremental form of the self-consistent method. The essence of the method is the realizable construction of the final composite from the matrix material through the successive replacement of an incremental volume of the current composite with that of the reinforcement. According to Dunn and Taya (1993), we have

$$\frac{\mathrm{d}\mathbf{M}_3(\lambda)}{\mathrm{d}\lambda}=\frac{1}{1-\lambda}[\mathbf{M}_1-\mathbf{M}_3(\lambda)]\mathbf{A}^{\mathrm{dif}}(\lambda) \tag{84}$$

where the fiber volume fraction λ is taken as a variable, $\mathbf{A}^{\mathrm{dif}}(\lambda)$ is computed as in the self-consistent method.

(4) *Mori–Tanaka method*. The key assumption in the Mori–Tanaka (1973) method is that a single inclusion is embedded in an infinite matrix subjected to an applied remote field equal to the as-yet-unknown averaged strain (stress) field in the matrix. According to Dunn and Taya (1993),

$$\mathbf{A}^{\mathrm{MT}} = \mathbf{A}^{\mathrm{dil}}[\lambda\mathbf{A}^{\mathrm{dil}} + (1-\lambda)\mathbf{I}]^{-1} \tag{85}$$

$\mathbf{A}^{\mathrm{dil}}$ in Eq. (85) is computed as in the dilute approximation.

8. Numerical results and comparison

In this section, a full numerical comparison of the developed generalized self-consistent method to other micromechanics methods are made. Hashin–Shtrikman's bounds are also used to examine the accuracy of various micromechanics methods.

Consider glass/epoxy composite with the constituent material properties:

$$E_1 = 72.4 \text{ GPa}, \quad v_1 = 0.2; \quad E_2 = 2.76 \text{ GPa}, \quad v_2 = 0.35 \tag{86}$$

where the subscripts 1 and 2 refer to the glass fiber and epoxy matrix, respectively.

By the well-known relations

$$B = \frac{E}{2(1+v)(1-2v)}, \quad G = \frac{E}{2(1+v)} \tag{87}$$

it is easy to obtain

$$B_1 = 50.3 \text{ GPa}, \quad G_1 = 30.2 \text{ GPa}; \quad B_2 = 3.41 \text{ GPa}, \quad G_2 = 1.02 \text{ GPa} \tag{88}$$

The variations of the effective in-plane bulk, in-plane shear and longitudinal shear moduli with the fiber volume fraction are plotted in Fig. 5, where the fiber aspect ratio $\gamma_1 = 0.3$ for various micromechanics methods and Hashin–Shtrikman's bounds are suitable for all shapes. It is seen that the predictions of the present method and Mori–Tanaka method are in excellent agreement. The self-consistent and differential methods (especially, the former) give much higher predictions, whereas the dilute approximation gives much lower predictions. It is not surprising considering the self-consistent method overestimates the inclusion interaction, whereas the dilute approximation ignores it. Form Fig. 5 it is also seen that in a large range of variations in the fiber volume fraction λ, the predictions by the dilute approximation fall outside Hashin–Shtrikman's lower bound. The results by the dilute approximation may be unacceptable. Some predictions by the self-consistent method fall outside Hashin–Shtrikman's upper bound, and the accuracy of the method is also suspicious.

By using the Mori–Tanaka method (1973), Huang and Hu's model (1995) and the present model, the variations of the in-plane bulk modulus and of the transverse shear modulus with fiber aspect ratio γ_1 are shown, respectively, in Fig. 6a and b for two different fiber volume fraction, $\lambda = 0.4$ and $\lambda = 0.6$. The three methods all indicate that as $\gamma_1 > 0.5$, γ_1 has little influence on the effective moduli. However, as $\gamma_1 < 0.5$, especially $\gamma_1 < 0.3$, it has a strong influence on the effective moduli. As $\gamma_1 > 0.5$, the three methods give almost identical effective shear modulus, whereas the Mori–Tanaka method gives slightly low shear modulus. As $\gamma_1 < 0.5$, Huang and Hu's model provides higher estimates of the effective moduli, and the series solution of the model diverges as $\gamma_1 < 0.1$. In the range of variations in the fiber aspect ratio of engineering composites, the results predicted by the present model and Mori–Tanaka method are in reasonable agreement. However, in the limit case of $\gamma_1 \to 0$, the two methods will give significantly different

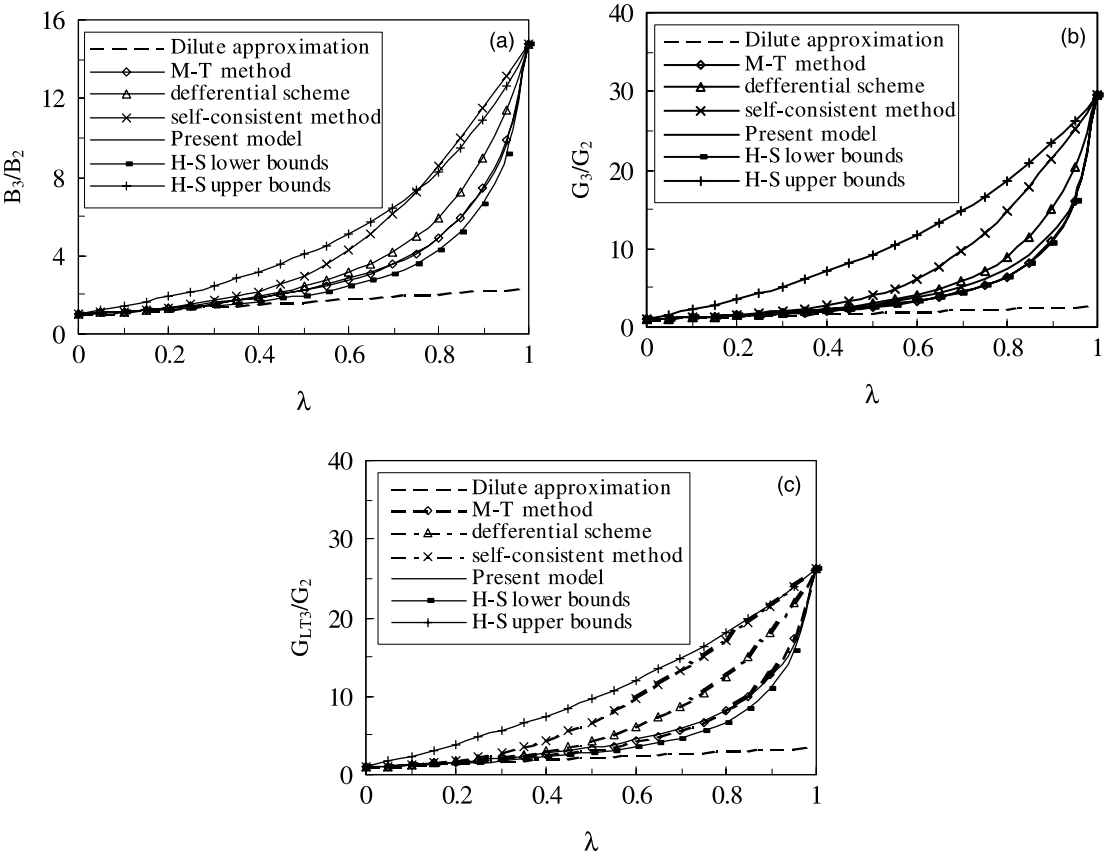

Fig. 5. Comparisons of micromechanics methods ($\gamma = 0.3$): (a) in-plane bulk modulus; (b) in-plane shear modulus; (c) longitudinal shear modulus.

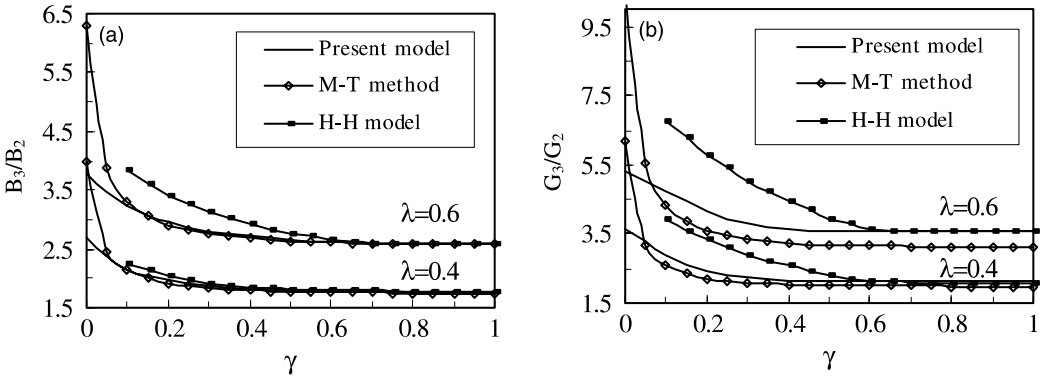

Fig. 6. Variations of in-plane effective moduli with aspect ratio γ: (a) in-plane bulk modulus; (b) in-plane shear modulus.

results. This is an open problem of theoretical interest yet, though it may fall outside practical application limits.

Numerical results show that the generalized self-consistent method is well suited for commonly countered range of fiber behavior. The method can provide reasonable results for a full range of variations in fiber aspect ratios (from circular fiber to ribbons) and for a complete spectrum of fiber volume fractions (from 0 to 1, and the latter limit case shows the correct asymptotic behavior in the fully packed case), for extreme types of the inclusion phase (from voids to rigid inclusions). Two extreme cases of fibers, i.e. tunnel voids and rigid fibers are taken as the illustrative examples: Fig. 7 shows the variations of the effective moduli with the aspect ratio of elliptical voids; Fig. 8 shows the variations of the effective moduli with the aspect ratio of rigid inclusions.

It is of interest to examine the sensitivity of the five effective material constants to the fiber section aspect ratio. Define aspect influence factors as

$$F_{\mathrm{B}} = \frac{B}{B_0}, \quad F_{\mathrm{GT}} = \frac{G_{\mathrm{T}}}{G_{\mathrm{T0}}}, \quad F_{\mathrm{EL}} = \frac{E_{\mathrm{L}}}{E_{\mathrm{L0}}}, \quad F_{\nu\mathrm{LT}} = \frac{\nu_{\mathrm{LT}}}{\nu_{\mathrm{LT0}}}, \quad F_{\mathrm{GLT}} = \frac{G_{\mathrm{LT}}}{G_{\mathrm{LT0}}} \tag{89}$$

where G_{T} denotes the transverse shear modulus, in instead of G in Sections 2–4, the subscript 0 refers to the value of the modulus for $\gamma = 1$, i.e. for the circular section fiber.

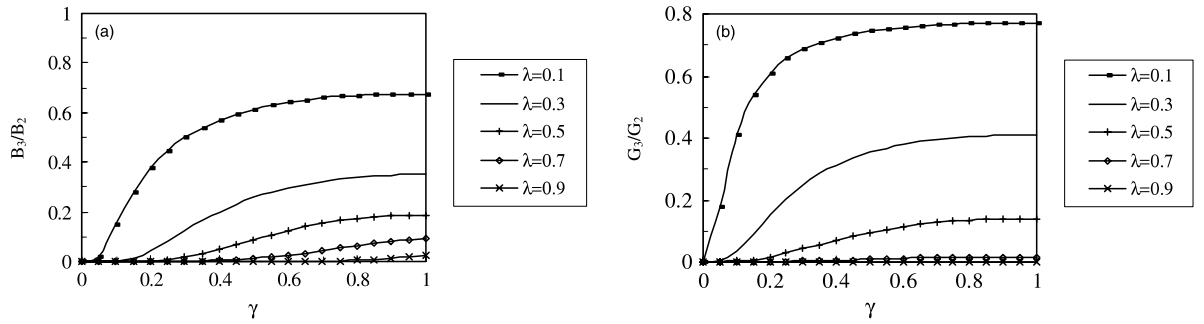

Fig. 7. Variations of in-plane effective moduli with aspect ratio γ for voids ($\nu_2 = 0.35$): (a) in-plane bulk modulus; (b) in-plane shear modulus.

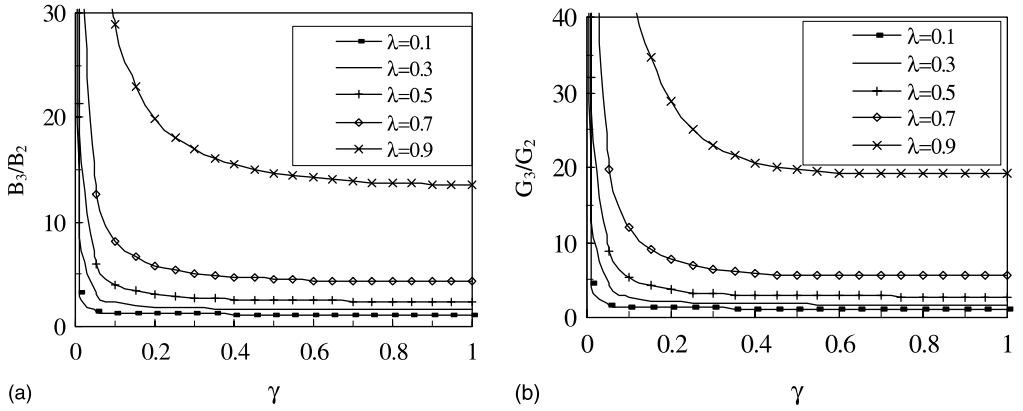

Fig. 8. Variations of in-plane effective moduli with aspect ratio γ for rigid fibers ($\nu_2 = 0.3$): (a) in-plane bulk modulus; (b) in-plane shear modulus.

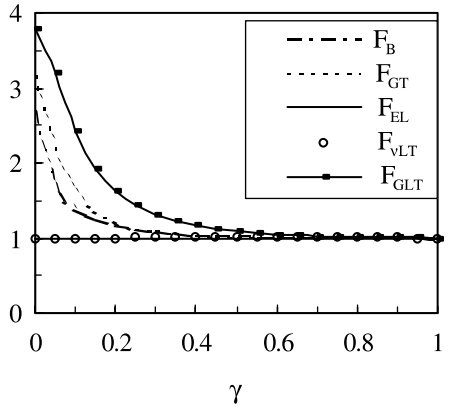

Fig. 9. Aspect influence factors of various effective moduli ($\lambda = 0.4$).

The variations of the aspect influence factors of the five material constants with the fiber section aspect ratio are plotted in Fig. 9, where the properties of the constituent materials are taken as

$$\lambda = 0.4, \quad E_1 = 413.69 \text{ GPa}, \quad v_1 = 0.2; \quad E_2 = 4.1369 \text{ GPa}, \quad v_2 = 0.35 \tag{90}$$

It is seen that the variations of various curves are very different. F_{EL} and $F_{v\mathrm{LT}}$ are almost horizontal curves, which indicate that the fiber shapes need not be considered in estimating the effective longitudinal tension modulus and major Poisson's ratio. F_{GLT} varies the most dramatically, which indicate that the aspect influence factor must be considered in estimating the effective longitudinal shear modulus.

Referring to Whitney and Riley (1966), experimental results on boron fiber reinforced composites indicate reasonable agreement with theory for longitudinal and transverse moduli, whereas very poor agreement with theory is obtained in the case of shear modulus. To yield reasonable predictions, semi-empirical equations, such as the widely used Halpin–Tsai equations (for example, see Jones and Devens, 1999) are introduced, where some constants must be determined by experiments. From Fig. 5 in Whitney and Riley (1966) it is observed that the shape of fiber section of the specimens are irregular, however, a theoretical model of circular section fiber is taken. The circular fiber model can provide accurate predictions for the longitudinal tensile modulus, but underestimates the effective longitudinal shear modulus. This is why their theoretical predictions for the latter are much lower than the experimental results. In fact, if the fiber section shape is taken as an equivalent ellipse with the aspect ration $\gamma \approx 0.4$, the theoretical predictions will be in reasonable agreement with the experiments.

9. Conclusion

A three-phase confocal elliptical cylinder model is proposed for fiber-reinforced composites. Based on this model, the generalized self-consistent method is extended to cover the case of elliptical section fibers oriented transversely randomly. The reasonableness of the fiber distribution function in the three-phase confocal elliptical cylinder model is shown.

Using the conformal mapping technique integrated with the Laurent series expansions, the analytical solutions for relevant plane strain, modified plane strain and longitudinal shear problems are obtained. The algebraic equations are established for predicting all the five effective moduli of fiber-reinforced composites, accounting for randomness in distribution and section orientation of fibers in a statistical sense.

The extended generalized self-consistent method provides convergent and reasonable results for a full range of variations in fiber section shape (from circular fibers to ribbons), for a complete spectrum of the fiber volume fraction (from 0 to 1, and the latter limit shows the correct asymptotic behavior in the fully packed case) and for extreme types of inclusion phases (from voids to rigid inclusions).

The dilute, self-consistent, differential and Mori–Tanaka methods are also extended to cover the case of transversely randomly oriented fibers. A comparison of the generalized self-consistent method with the four micromechanics methods and with Hashin–Shtrikman's bounds is made. It is seen that the generalized self-consistent method and Mori–Tanaka method provide very close predictions, whereas other method, especially the dilute approximation and self-consistent method, lead to significant deviations. Most predictions by the dilute approximation and some predictions by the self-consistent method fall outside Hashin–Shtrikman's bounds, and the accuracy of the two methods (especially the former) are suspicious.

A very different dependence of the five effective moduli on fiber section shape is theoretically predicted, and it provides a reasonable explanation on the poor correlation between previous theory and experiment in the case of longitudinal shear modulus. Such a study is of importance in improving accuracy in micromechanics predictions.

The three-phase confocal elliptical cylinder model can also serve as an inclusion/interphase layer/matrix model, in terms of which, the stress concentration in such microstructures can be investigated (refer to Ru et al., 1999; Wu and Du, 2000; Jiang and Cheung, 2001). This work will be left for readers.

Acknowledgements

The work is supported by the Hong Kong Research Grants Council, the National Natural Science Foundation of China and the Aviation Science Foundation of China. The authors would like to thank Professor G.K. Hu for his valuable proposal for Section 6.

Appendix A. The algebraic equation to determine the expansion coefficients of the complex potentials

$$\left(\frac{p_{12}}{\rho_1^{2m}}-s_{12}\frac{m}{\rho_1^2}\right)a_m-s_{12}b_m-\frac{p_{22}}{\rho_1^{2m}}c_{-m}-s_{12}\left(\rho_1^2+\frac{1}{\rho_1^2}\right)\sum_{k=m+2,m+4}^{2M-1}ka_k=0 \tag{A.1}$$

$$(p_{12}\rho_1^{2m}-s_{12}m\rho_1^2)a_m-s_{12}b_m-p_{22}\rho_1^{2m}c_m-s_{12}\left(\rho_1^2+\frac{1}{\rho_1^2}\right)\sum_{k=m+2,m+4}^{2M-1}ka_k=0 \tag{A.2}$$

$$\begin{aligned}&\left(\frac{q_{21}}{\rho_1^{2m}}+p_{21}\frac{m}{\rho_1^2}\right)a_m+p_{21}b_m-p_{22}\frac{m}{\rho_1^2}c_m-p_{22}d_m-\left[\frac{q_{21}}{\rho_1^{2m+4}}-p_{21}(m+2)\rho_1^2\right]a_{m+2}-p_{21}b_{m+2}\\&\quad-p_{22}(m+2)\rho_1^2c_{m+2}=0\end{aligned} \tag{A.3}$$

$$\begin{aligned}&\left(q_{21}\rho_1^{2m}-p_{21}\frac{m}{\rho_1^2}\right)a_m+p_{21}b_m+p_{22}\frac{m}{\rho_1^2}c_{-m}-p_{22}d_{-m}-[q_{21}\rho_1^{2m-4}+p_{21}(m-2)\rho_1^2]a_{m-2}-p_{21}b_{m-2}\\&\quad+p_{22}(m-2)\rho_1^2c_{-(m-2)}=0\end{aligned} \tag{A.4}$$

$$p_{32}\frac{m}{\rho_2^2}c_m+\frac{q_{32}}{\rho_2^{2m}}c_{-m}+p_{32}d_m+p_{32}(m+2)\rho_2^2c_{m+2}+\frac{q_{32}}{\rho_2^{2m+4}}c_{-(m+2)}=\delta_{1m}p_{33}\left(\frac{e_1}{\rho_2^2}+f_1\right) \tag{A.5}$$

$$p_{23}\rho_2^{2m}c_m + s_{23}\frac{m}{\rho_2^2}c_{-m} - s_{23}d_{-m} - p_{23}\rho_2^{2m-4}c_{m-2} + s_{23}(m-2)\rho_2^2 c_{-(m-2)} + \delta_{1m}\left\{\frac{p_{23}}{\rho_2^2}c_{-1} - s_{23}\left[\frac{1}{\rho_2^2}c_1 + \sum_{k=1,3}^{2M-1} d_k + \left(\rho_2^2 + \frac{1}{\rho_2^2}\right)\sum_{k=3,5}^{2M-1} kc_k\right]\right\} = \delta_{1m}p_{33}\rho_2^2 e_1 - \delta_{3m}p_{33}\rho_2^2 e_1 \tag{A.6}$$

where $m = 1, 3, \ldots, 2M-1$, which leads to $6M$ equations; p_{ij}, q_{ij} and s_{ij} refer to Eq. (52); $a_{-1} = a_1$, the unknown coefficients with a subscript larger than $2M-1$ are taken as zero; δ_{ij} is the Kronecker notation

$$\delta_{ij} = \begin{cases} 0, & i \neq j \\ 1, & i = j \end{cases} \tag{A.7}$$

References

Benveniste, Y., 1985. The effective mechanical behavior of composite materials with imperfect contact between the constituents. Mech. Mater. 4, 197–208.

Christensen, R.M., Lo, K.H., 1979. Solutions for effective shear properties in three phase sphere and cylinder models. J. Mech. Phys. Solids 27, 315–330, 34 (6) (1986) 639.

Christensen, R.M., 1990. A critical equation for a class of micromechanics models. J. Mech. Phys. Solids 38, 379–404.

Christensen, R.M., Schantz, H., Shapiro, J., 1992. On the range of validity of the Mori–Tanaka method. J. Mech. Phys. Solids 40 (1), 69–73.

Christensen, R.M., 1993. Effective properties of composite materials containing voids. Proc. R. Soc. Lond. A 440, 461–473.

Dunn, M.L., Taya, M., 1993. Micromechanics predictions of the effective electroelastic moduli of piezoelectric composites. Int. J. Solids Struct. 30 (2), 161–175.

Eshelby, J.D., 1957. The determination of the elastic field of an ellipsoidal inclusion, and related problems. Proc. R. Soc. Lond. A 241, 376–396.

Hashin, Z., Shtrikman, S., 1963. A variational approach to the theory of the elastic behavior of multi-phase materials. J. Mech. Phys. Solids 11, 127–140.

Hu, G.K., Weng, G.J., 2000a. The connections between the double-inclusion model and the Ponte Castaneda–Willis, Mori–Tanaka, and Kuster–Toksoz models. Mech. Mater. 32, 495–503.

Hu, G.K., Weng, G.J., 2000b. Some reflections on the Mori–Tanaka and Ponte Castaneda–Willis methods with randomly oriented ellipsoidal inclusions. Acta. Mech. 140, 31–40.

Huang, Y., Hu, K.X., Chandra, 1994. A generalized self-consistent mechanics method for microcracked solids. J. Mech. Phys. Solids 42, 1273–1291.

Huang, Y., Hu, K.X., 1995. A generalized self-consistent mechanics method for solids containing elliptical inclusions. Trans. ASME 62, 566–572.

Jiang, C.P., Cheung, Y.K., 1998. A fiber/matrix/composite model with a combined confocal elliptical cylinder unit cell for predicting the effective longitudinal shear modulus. Int. J. Solids Struct. 35 (30), 3977–3987.

Jiang, C.P., Cheung, Y.K., 2001. An exact solution for the three-phase piezoelectric cylinder model under antiplane shear and its applications to piezoelectric composites. Int. J. Solids Struct. 38, 4777–4796.

Jiang, C.P., Tong, Z.H., Cheung, Y.K., 2001. A generalized self-consistent method for piezoelectric fiber reinforced composites under antiplane shear. Mech. Mater. 33, 295–308.

Jones, R.M., Devens, K.S., 1999. Mechanics of Composite Materials. Taylor Francis, London.

Luo, H.A., Weng, G.J., 1987. On Eshelby's inclusions problem in a three-phase spherically concentric solid, and a modification of Mori–Tanaka's method. Mech. Mater. 6, 347–361.

Muskhelishivili, N.I., 1975. Some Basic Problems of Mathematical Theory of Elasticity. Noordhoff, Leyden.

Mori, T., Tanaka, K., 1973. Average stress in matrix and average elastic energy of materials with misfiting inclusions. Acta Metall. 21, 571–574.

Norris, A.N., 1985. A differential scheme for the effective moduli of composites. Mech. Mater. 4, 1–16.

Riccardi, A., Montheilet, F., 1999. A generalized self-consistent method for solids containing randomly oriented spheroidal inclusions. Acta Mech. 133, 39–50.

Ru, C.Q., Schiavone, P., Mioduchowski, A., 1999. Uniformity of stresses within a three-phase elliptic inclusion in anti-plane shear. J. Elasticity 52, 121–128.

Taya, M., Chou, T.W., 1981. On two kinds of ellipsoidal inhomogeneities in an infinite elastic body: an application to a hybrid composite. Int. J. Solids Struct. 17, 553–563.

Whitney, J.M., Riley, M.B., 1966. Elastic properties of fiber reinforced composite materials. AIAA J. 4 (9), 1537–1542.

Wu, L.Z., Du, S.Y., 2000. A rigid line in a confocal elliptic piezoelectric inhomogeneity embedded in an infinite piezoelectric medium. Int. J. Solids Struct. 37, 1453–1469.

Zhao, Y.H., Weng, G.J., 1990. Effective elastic moduli of ribbon-reinforced composites. ASME J. Appl. Mech. 57, 158–167.